Hindawi
Complexity
Volume 2018, Article ID 2494509, 10 pages
https://doi.org/10.1155/2018/2494509

WILEY | Hindawi

Research Article

Atmospheric Dynamics Leading to West European Summer Hot Temperatures Since 1851

M. Carmen Alvarez-Castro, Davide Faranda, and Pascal Yiou

Laboratoire des Sciences du Climat et de l'Environnement, UMR 8212 CEA-CNRS-UVSQ, IPSL, Université Paris-Saclay, 91191 Gif-sur-Yvette, France

Correspondence should be addressed to M. Carmen Alvarez-Castro; carmen.alvarez-castro@lsce.ipsl.fr

Received 18 August 2017; Accepted 22 November 2017; Published 16 January 2018

Academic Editor: Peter Giesl

Summer hot temperatures have many impacts on health, economy (agriculture, energy, and transports), and ecosystems. In Western Europe, the recent summers of 2003 and 2015 were exceptionally warm. Many studies have shown that the genesis of the major heat events of the last decades was linked to anticyclonic atmospheric circulation and to spring precipitation deficit in Southern Europe. Such results were obtained for the second part of the 20th century and projections into the 21st century. In this paper, we challenge this vision by investigating the earlier part of the 20th century from an ensemble of 20CR reanalyses. We propose an innovative description of Western-European heat events applying the dynamical system theory. We argue that the atmospheric circulation patterns leading to the most intense heat events have changed during the last century. We also show that the increasing temperature trend during major heatwaves is encountered during episodes of Scandinavian Blocking, while other circulation patterns do not yield temperature trends during extremes.

1. Introduction

In Western Europe, recent hot summers were characterized by anomalous meteorological conditions. In those situations, such as 2003, the heat was prolonged and intense, and the consequences were disastrous for society and ecosystems [1–5].

European surface temperature variations are influenced by processes that combine radiative forcing, the large-scale atmospheric circulation, and local phenomena. Over the last five decades, most of the intense European heat events have been connected to prolonged spells of anticyclonic circulation (Scandinavian blocking) and dry spring conditions in Southern Europe [6–11]. However, the summer of 2011 was cool and preceded by a dry spring; the summer of 2013 was warm and preceded by a wet spring; and the summer of 2015 was warm with persisting southerly atmospheric flows and no lasting blocking episodes [12]. The goal of this paper is to assess the robustness of the link between heat events and atmospheric circulation. We perform a statistical and dynamical analysis on a long period that covers 1851–2014. Since anticyclones extend to a radius of few hundreds kilometers, such a connection must be investigated on a regional scale [13, 14]. Hence, we restrict our analysis to Western Europe in the region covering France and the Iberian Peninsula, whose weather conditions are strongly influenced by the atmospheric circulation over the North Atlantic. This analysis also puts some of the results of Horton et al. [15] on this link into a broader time perspective.

2. Data and Methods

We base our analysis on the sea-level pressure (SLP) and the surface temperature fields during summers (June-July-August: JJA) in 20th Century Reanalysis data version 2c (20CRv2c: 1851–2014, [16]) with 2° of resolution and bias correction applied in the sea-ice distribution by assimilating new SST and sea-ice cover (SIC) data (Hirahara et al. 2014). To ensure the robustness of the results, we used the ensemble mean (EM) and the 56 members of the ensemble. The analysis is completed with other reanalysis products: NCEP (1948–2016) [17] and ERA20C reanalysis (1900–2000)

[18] (see supplementary material). In order to describe the variability of the atmospheric circulation, we decompose the summer SLP anomalies field (obtained by removing the seasonal cycle) into four weather regimes following the approach of Yiou et al. [19] and study their connection with heat events at seasonal (i) and subseasonal (ii) timescales in Western Europe [10°W–7.5°E; 35–50°N]: (i) Seasonal: the 24 summers with high mean temperature anomalies (with respect to the climatology) of the period 1851–2014, and (ii) subseasonal: heatwaves defined as periods with high temperatures anomalies for at least five consecutive days. In both analyses temperatures are detrended by removing a linear trend calculated from the time series of summer seasonal means. The goal of the detrending is to remove the effect of the well-documented European temperature increase, which does not depend on the weather pattern.

2.1. Weather Regimes. Weather regimes are recurring states of the atmospheric circulation and provide a useful description of the atmospheric variability [20, 21]. Following the methods of Michelangeli et al. [20] and Yiou et al. [19], we compute four weather regimes ($k = 4$) over the North-Atlantic region [80°W–50°E; 20–70°N] (Figures 1(a)–1(d)) on daily NCEP SLP anomalies (reference period: 1970–2010) over the summers (June-July-August: JJA). We take the first ten Empirical Orthogonal Functions (EOFs) of SLP anomalies (with weights that are proportional to the cosine of latitude) and the corresponding Principal Components (PCs). Then we perform a classification, with a k-means algorithm [20], and a choice of four weather regimes. This classification is iterated several times with random initial conditions following the procedure of Yiou et al. [19] in order to obtain weather regimes that are stable. The choice of four weather regimes is to be consistent with the seminal paper of [22]. For comparison, we classify different reanalysis datasets with the NCEP weather regimes. All the reanalysis data are interpolated onto the NCEP grid ($2.5° \times 2.5°$). The SLP data classifications of all reanalyses are obtained by determining the minimum of the Euclidean distances to the four NCEP summer weather regime centroids. This is achieved without further EOF truncation. The NCEP summer weather regimes are shown in Figures 1(a)–1(d), with the same nomenclature as in Cassou et al. [22]: (a) the negative phase of North-Atlantic Oscillation (NAO−) showing a dipole between Greenland and Northern Europe, (b) the Atlantic Ridge (AR), with a high pressure over the center of the North Atlantic and some common features with the positive phase of NAO, (c) Scandinavian Blocking (BLO), with a high pressure center over Scandinavia, and (d) Atlantic Low (AL), with a low pressure center covering the central North Atlantic.

To ensure that there are no inhomogeneities in the method, we have verified that the root mean square error (RMSE) between the reference period and the other periods/datasets is small (Figure S1 and Table S1).

2.2. Projection onto Weather Regimes for a Dynamical Representation. In order to visualize the dependence between the daily SLP fields and the four weather regimes, we represent the *trajectory* of each summer in the space of correlations using an approach based on dynamical systems theory [23]. In this framework, the motion of a particle is represented in the space defined by its position and speed (the so-called phase space). In our set-up, the particle is replaced by a SLP field and the directions in phase space correspond to the projections on the four weather regimes. Trajectories provide additional information with respect to the monthly average statistical quantities, on the time dependence and the coherence of the dynamical projection with respect to weather regime bases. If a trajectory jumps every day to a different region of the phase space, then a dominant weather regime is not representative of the dynamical behavior of events lasting several days. If instead the trajectory occupies a restricted region of the phase space with smooth transitions of the projection among weather regimes, then the dynamical representation is informative and the base of weather regimes is appropriate.

This is equivalent to assuming the existence of a low-dimensional attractor. The caveat is that the weather regime description is a first-order simplification of the atmospheric circulation that captures large-scale features. Although this phase-space method has been debated since Lorenz [24], there is theoretical [25] and experimental [26] evidence that such a procedure is effective when the dynamics can be projected on a low-dimensional phase space with a stochastic perturbation.

3. Results and Discussion

The link between the North-Atlantic atmospheric circulation and heat events over France and the Iberian Peninsula is investigated at short and long timescales. Both timescales carry a physical and societal relevance.

3.1. Seasonal Scale: Weather Regimes during the Warmest Summers. We carried out a statistical analysis of the hottest summers of the period 1851–2014 using 56 members and the ensemble mean (EM) of the 20CRv2c. In Western Europe [10°W–7.5°E; 35–50°N], the 24 warmest summers (Figures 1(e) and 1(f)) are defined in each dataset as the ones having the highest average temperature anomalies with respect to the climatology. Figure 1(e) shows the probability to have a dominant weather regime, which is the one with the highest anomalous frequency, in each summer detected. From the selection of the 24 warmest summers for each member, we detect 52 different summers. In order to show the agreement between the members, we calculate the probability to have a summer dominated by each weather regime (Figure 1(e)). We divide the number of members that detects a weather regime dominating that summer by the total number of members that has detected that summer as a warm summer. For instance, we find that for 30 members, the summer of 1887 is one of the 24 warmest summers. For 21 of those 30 members NAO− is the dominant weather regime and BLO for the other 9 members. However, we find a total agreement within 51 members detecting 2003 as a warmer summer with AL as the unique weather regime dominating the summer. Hence, as Figure 1(e) shows, there is a higher probability to find a total agreement within the members after 1950, being mainly

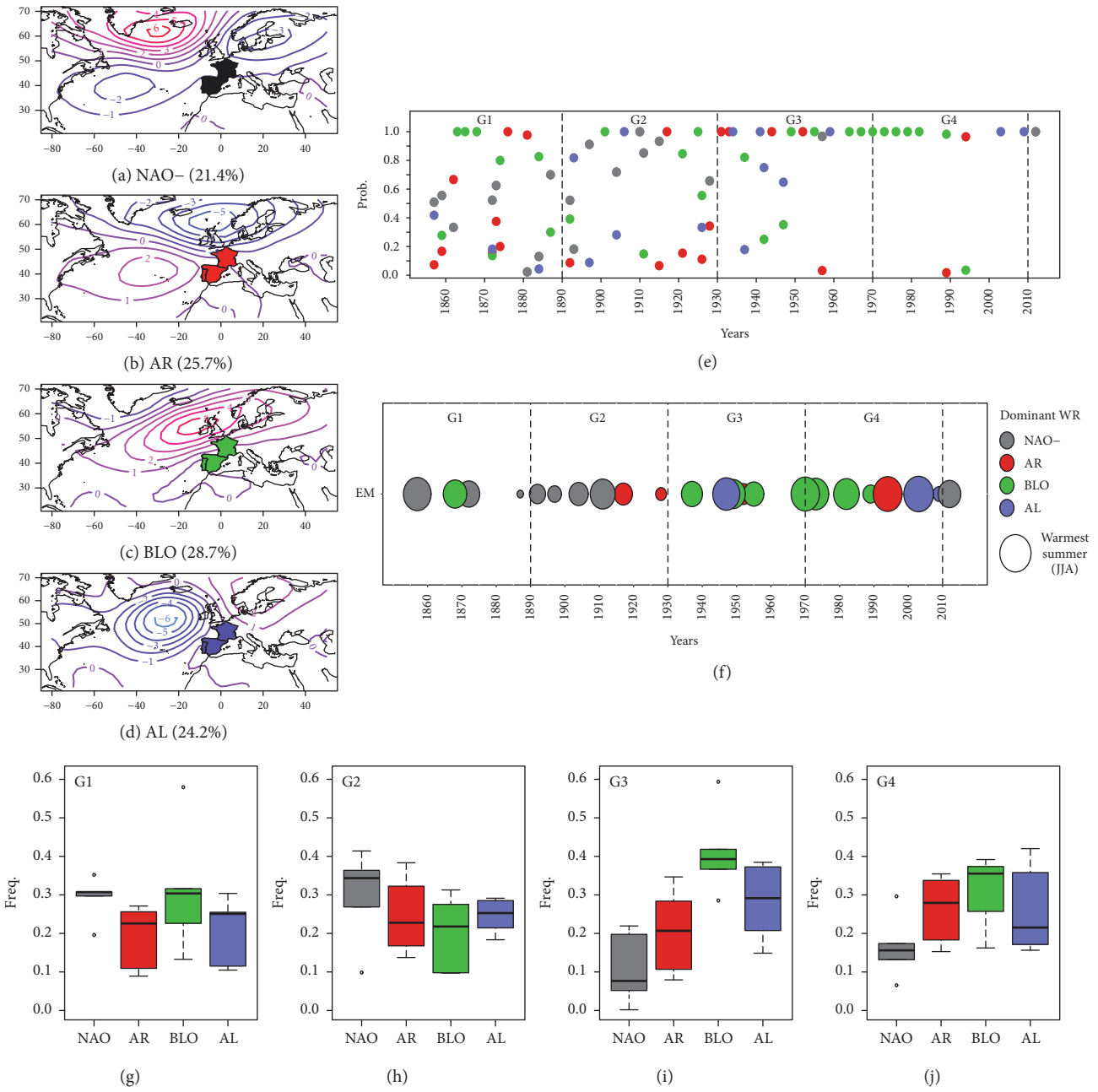

FIGURE 1: Summer SLP weather regimes over the North-Atlantic region and their dominance in the twenty warmest summers during 1871–2011 in Western Europe. (a)–(d) Summer SLP (hPa anomalies) weather regimes. (a) North-Atlantic oscillation in its negative phase (NAO−). (b) Atlantic Ridge (AR). (c) Blocking (BLO). (d) Atlantic Low (AL) weather regime. (e) Probability to find a dominant weather regime in all the warmest summers (EM and 56 members). (f) 24 warmest summers in Western Europe (colored region in (a)–(d)) with their dominant weather regime (20CRv2c EM). Circle size depends on temperature (anomalies), the largest the warmest. Colors represent the dominant weather regime for each summer based on the highest anomalous frequency. (g)–(j) Boxplots of daily weather regimes during the 24 warmest summers of 20CRv2c EM (as in (f)) in Western Europe separated by groups of 6 summers per 40 years: (g) shows group G1, (h) group G2, (i) group G3, and (j) group G4 1.

BLO the dominant regime of warmest summers during the second half of the 20th century and also briefly during the end of the 19th century. NAO− and AR are the most dominant regimes during the first half of the 20th century. This is also evident when we study the EM (Figures 1(f)–1(j)). Figure 1(f) shows the dominant weather regime (colors) for the warmest summers (circle size) of the EM (20CRv2c, see Figure S2(i) of supplementary material for NCEP, ERA20C, and 20CR and Figure S3 for some examples of warmest summers). We have divided the warmest summers detected (vertical bars and Figures 1(g)–1(j)) in 4 groups, in order to study the variability during short periods of 30 years. Boxplots

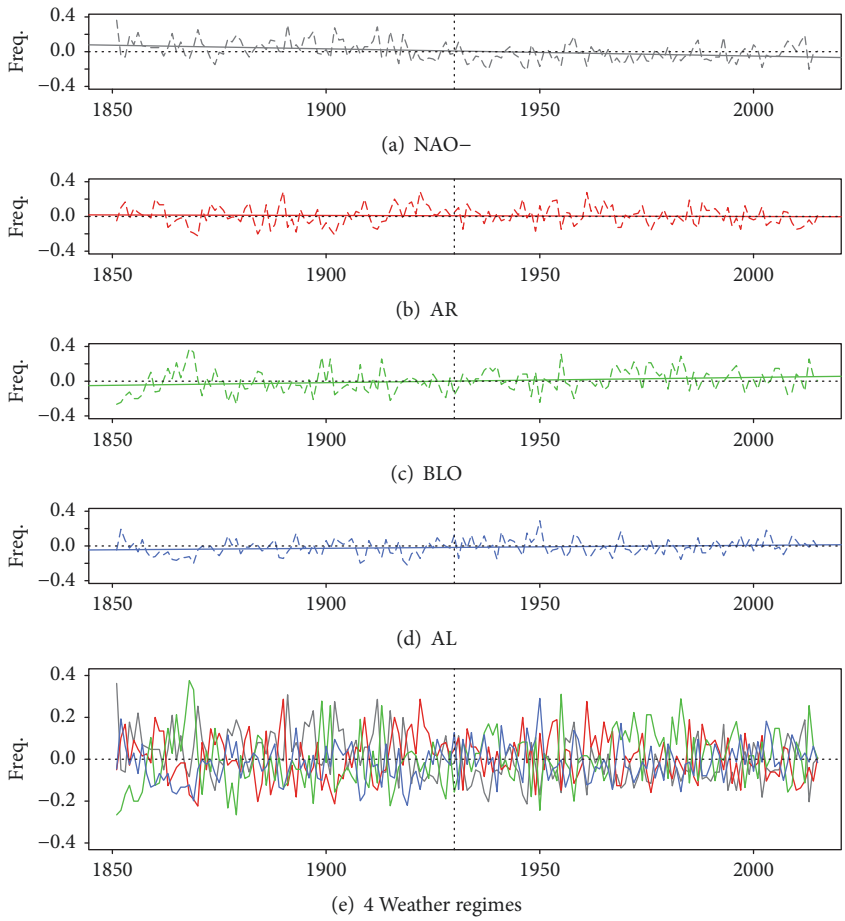

Figure 2: Relative long-term summer weather regime frequency. Relative frequency of summer SLP (hPa) weather regimes over the North-Atlantic region (1851–2014) using 20CRv2c. Here we show SLP anomalies with respect to the reference period 1970–2010 for each (a)–(d) and all (e) weather regimes; solid lines in (a)–(d) represent the linear trend for each regime. 1930 is marked with a vertical dashed line.

in Figures 1(g)–1(j) indicate the daily frequency of weather regimes by group. In groups G1 (Figure 1(g)), G3 (Figure 1(j)), and G4 (Figure 1(j)), BLO is the most frequent regime during warmest summers, while in group G2 NAO− and AR are the most representatives ones. Most of the warmest summers (largest circles in Figure 1(f)) occur during the second part of the 20th century. As observed by Stott et al. [27] and Meehl and Tebaldi [28], they also increase in frequency over time.

Figures 2(a)–2(e) (Figures S2(a)–S2(d) for NCEP and Figures S2(e)–S2(h) for ERA20C) show the anomalous summer frequency of weather regimes in EM of 20CRv2c with respect to the NCEP reference period. In this figure, we see that NAO− is the unique regime decreasing in frequency with the time, and BLO is the one increasing in frequency with the time (see also Figures S4 and S5).

To understand such trends, we decompose the average information found with the statistical analysis via the dynamical representation of the warmest summers (Figure 3 and S6), defined in Section 2.2. We project the daily SLP anomaly fields (grey lines) onto the 4 weather regimes (NAO− and AR regimes in Figures 3(a), 3(c), 3(e), and 3(g) and BLO and AL regimes in Figures 3(b), 3(d), 3(f), and 3(h)). This analysis synthesizes the trajectory of the atmospheric circulation during heat events (colors) in a space represented by the weather regimes. Circles in the axes represent the average correlations of the warmest summers.

Consistently with the previous analysis, we find that the atmospheric dynamics has evolved from patterns that are positively correlated with NAO− during the late 19th century and the beginning of the 20th century (groups G1 and G2, Figures 3(a) and 3(c)), to negative correlations during the rest of the record (Figures 3(e) and 3(g)). Similar projections on BLO and AL regimes show that BLO has the opposite change of NAO− (mainly in groups G2 and G3), being negative during the early period of 20th century (Figure 3(d)) and positive during the middle and late 20th century (Figures 3(f)–3(h)). AR and AL regimes do not show significant differences between the periods. Those correlations add daily temporal information and highlight a change of atmospheric behavior. Thus, the dominant weather regime is a valid concept as the trajectories of heatwaves persist at subseasonal scales around the same region of the phase space. These changes are consistent within the 20CRv2c ensemble, as the analysis of the 56 members (Figure 4(a)) shows consistent results with the EM. In Figure 4, we represent the average correlations of warmest summers as for Figure 3 (circles in the axes) but for

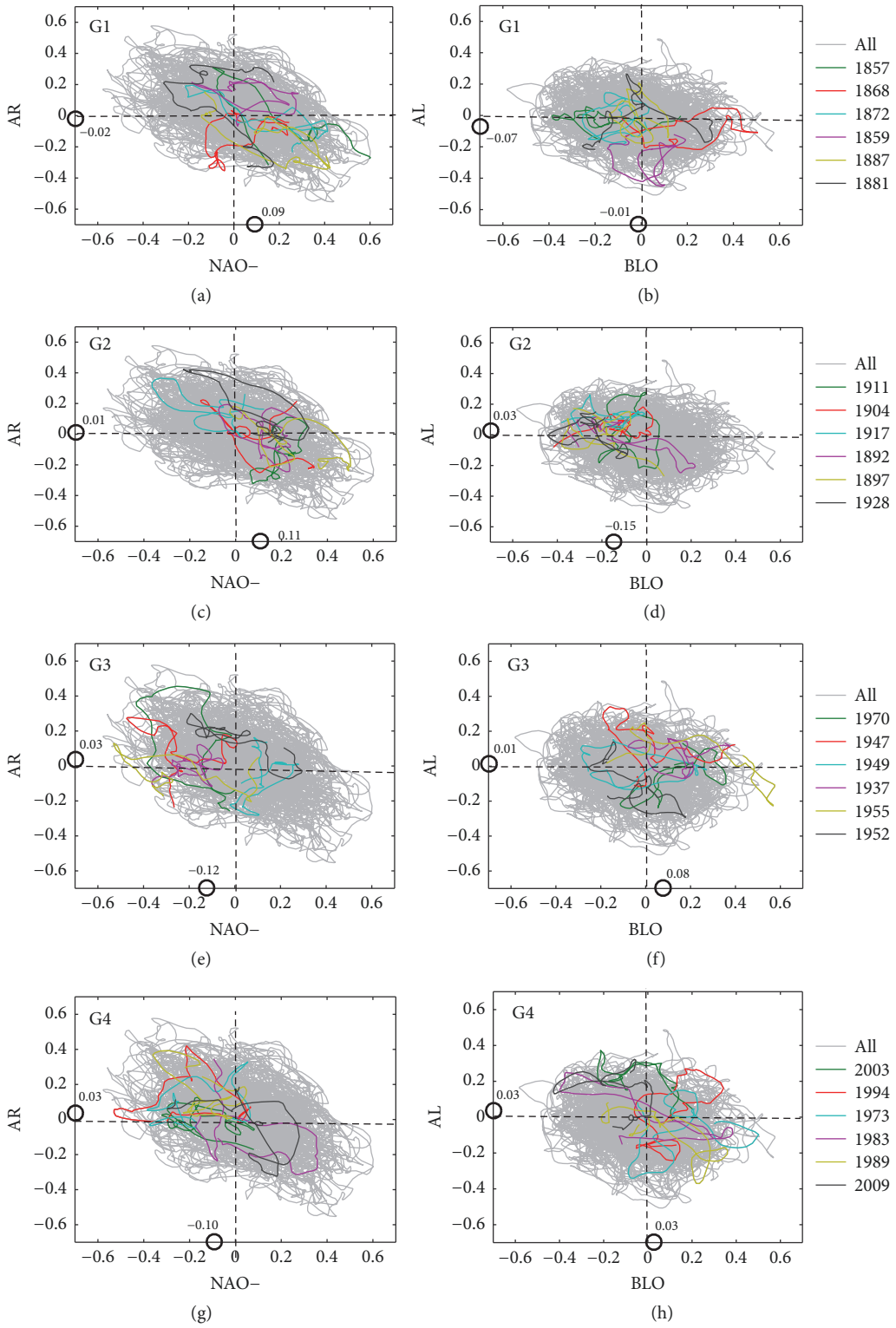

FIGURE 3: Dynamical representation of the warmest summers. Correlations of daily SLP fields and NAO− (x-axis), AR (y-axis) (top) and AL, BLO (bottom) weather regimes for the 4 groups of summers. Warmest summers are colored as in the legend with light grey lines representing all data. Average correlations of warmest summers with respect to the NAO− weather regimes (black circle on x-axis). A moving average filter of 30-day window was applied to the warmest summers for better representation.

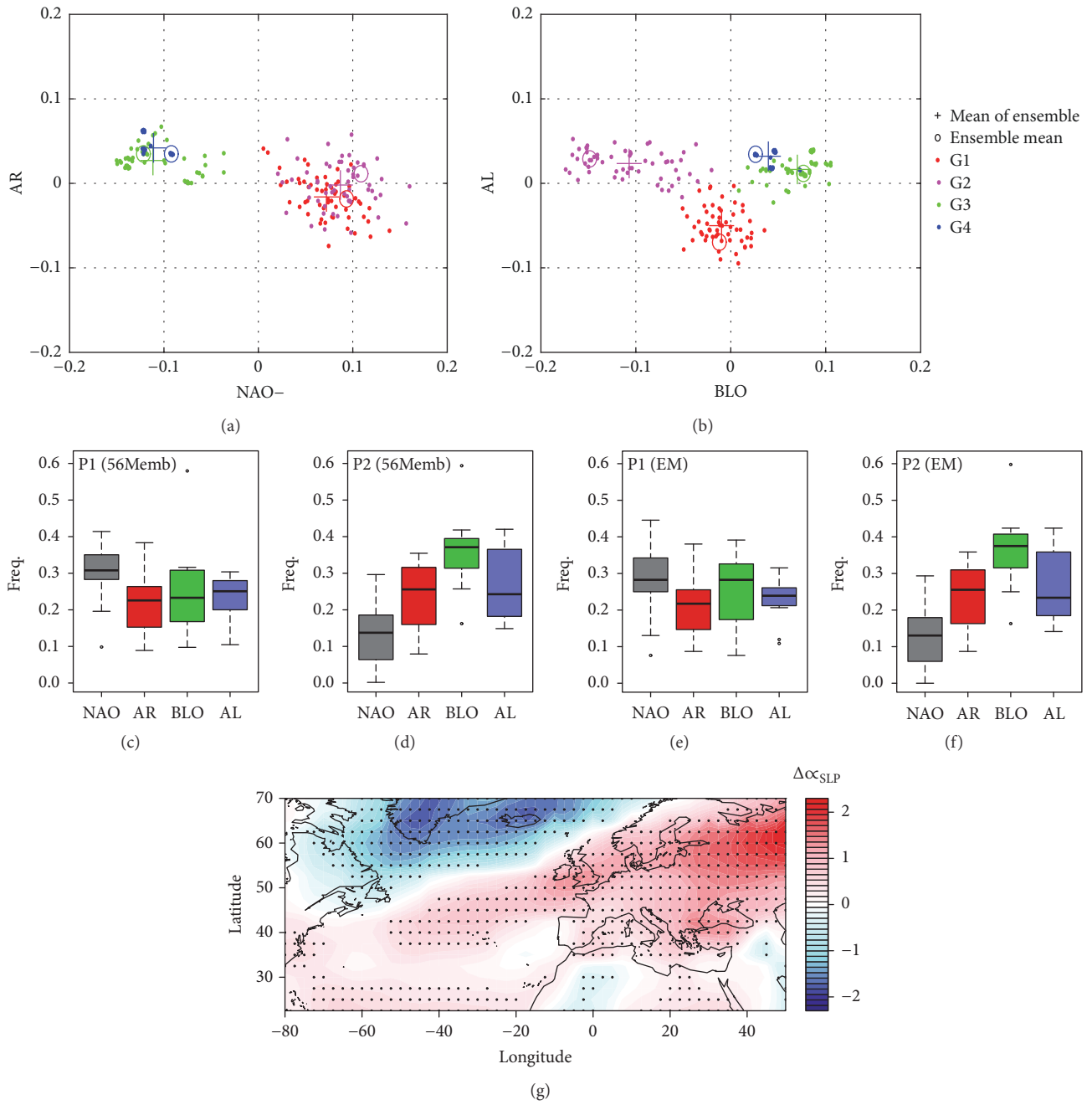

FIGURE 4: Changes in the dynamical representation of the warmest summers. (a, b) Average correlations of warmest summers with respect to the 4 weather regimes (black circle on x-axis in Figure 3), points represent each member, crosses represent the mean of all the 56 members, and circles represent the EM. Colors represent the 4 groups of summers (G1 red, G2 purple, G3 green, and G4 blue). In (c)–(f), boxplots show frequencies of the 4 weather regimes classified in two periods: (c, e) for summers before 1930 (groups G1 + G2) and (d, f) for summers after 1930 (groups G3 + G4), for all the 56 members (c, d) and the EM (e, f). (g) shows the difference in the SLP mean between those two periods (after 1930 and before 1930). Points represent significance at 95 percent after the performance of a Monte Carlo test.

all the 56 members and the EM. Therefore, if we study now the daily frequency of weather regimes classifying the warmest summers by only two periods, before (P1) and after (P2) 1930, we find similar results as in Figures 3 and 4(a), opposite frequencies between NAO− and BLO. Higher frequencies of NAO− are detected in P1 for 56 members (Figure 4(c)) and the EM (Figure 4(e)), and higher frequencies of BLO are detected in P2 for 56 members (Figure 4(d)) and the EM (Figure 4(f)).

To complement this weather regimes analysis, we compute the difference of the mean SLP for EM between these two periods during the warmest summers: $\Delta_{SLP} = \mu_{SLP(P2)} - \mu_{SLP(P1)}$. We obtain a BLO regime pattern (Figure 4(g)) using the EM or 56 members (not shown here). This means that it

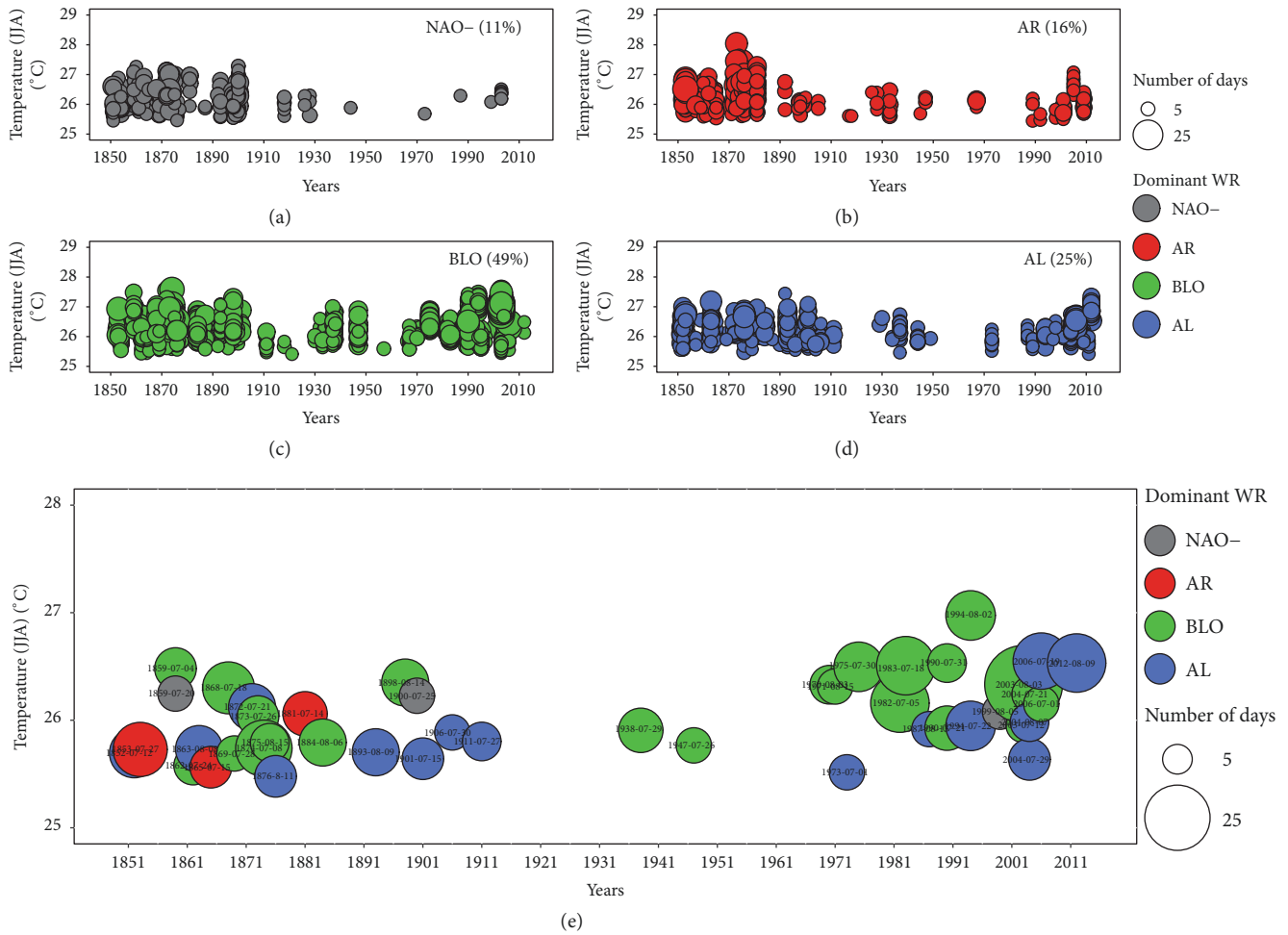

Figure 5: Dominant weather regimes during summer heatwave events. In (a)–(d), summer heatwave events (95th percentile) for all the members and (e) EM (circles with stars) of 20CR data, 1851–2014. Colors correspond to the dominant weather regime in each event, temperature (y-axis) and years (x-axis). Circle sizes depend on the event duration by number of days, the larger the longer duration.

is the most representative pattern for the period P2, being the period P1 similar to the NAO–.

Therefore, our analysis shows significant changes in the dominating weather regimes associated with the warmest summers. If BLO is dominant from the second part of 20th century, scarce occurrences of this weather regime are found before 1930, with the exception of a small period at late 19th century, even within the ensemble members of 20CRv2c. These results reflect a change in the regime frequencies and dominance conducing to warm extremes in a multidecadal scale due to, most likely, an internal variability. BLO and AL regimes are conducive to warm extremes and NAO– and AR are the opposite [22]. We found that, after 1930, it is more frequent to find the hottest summers linked to what we know as warm regimes. BLO (the most frequent one after 1930) leads to stagnant air and potential land-surface feedback, whereas AL relies on advection from lower latitudes. On the other hand, NAO– is the dominant weather regime during the warmest summers up to 1930. This weather regime contributes to a weakening of the westerly flow from the Atlantic into Western Europe. AR regime is more stable in time.

3.2. Subseasonal Scale: Weather Regimes during Heatwave Events. To understand whether those results hold also for short time events (at least 5 consecutive days), independently from the fact that they have been observed during hot summers, we compute the average temperature during heatwaves striking Western Europe.

Heatwave events are defined when the summer temperature exceeds a threshold based on percentiles (P90, P95) for more than 5 consecutive days. Figure 5 shows heatwave events above the P95 threshold, computed on the area temperature anomalies (mean of France and the Iberian Peninsula) for the 56 members (Figures 5(a)–5(d)) and for the EM (Figure 5(e)) (see Figure S7 of supplementary material). Temperatures in Figure 5 are average values during each heatwave event. Heatwaves events are grouped by the dominating weather regime. We find that 11% of total events are dominated by NAO– (Figure 5(a)), 49%, by BLO (Figure 5(c)). Heatwaves that are

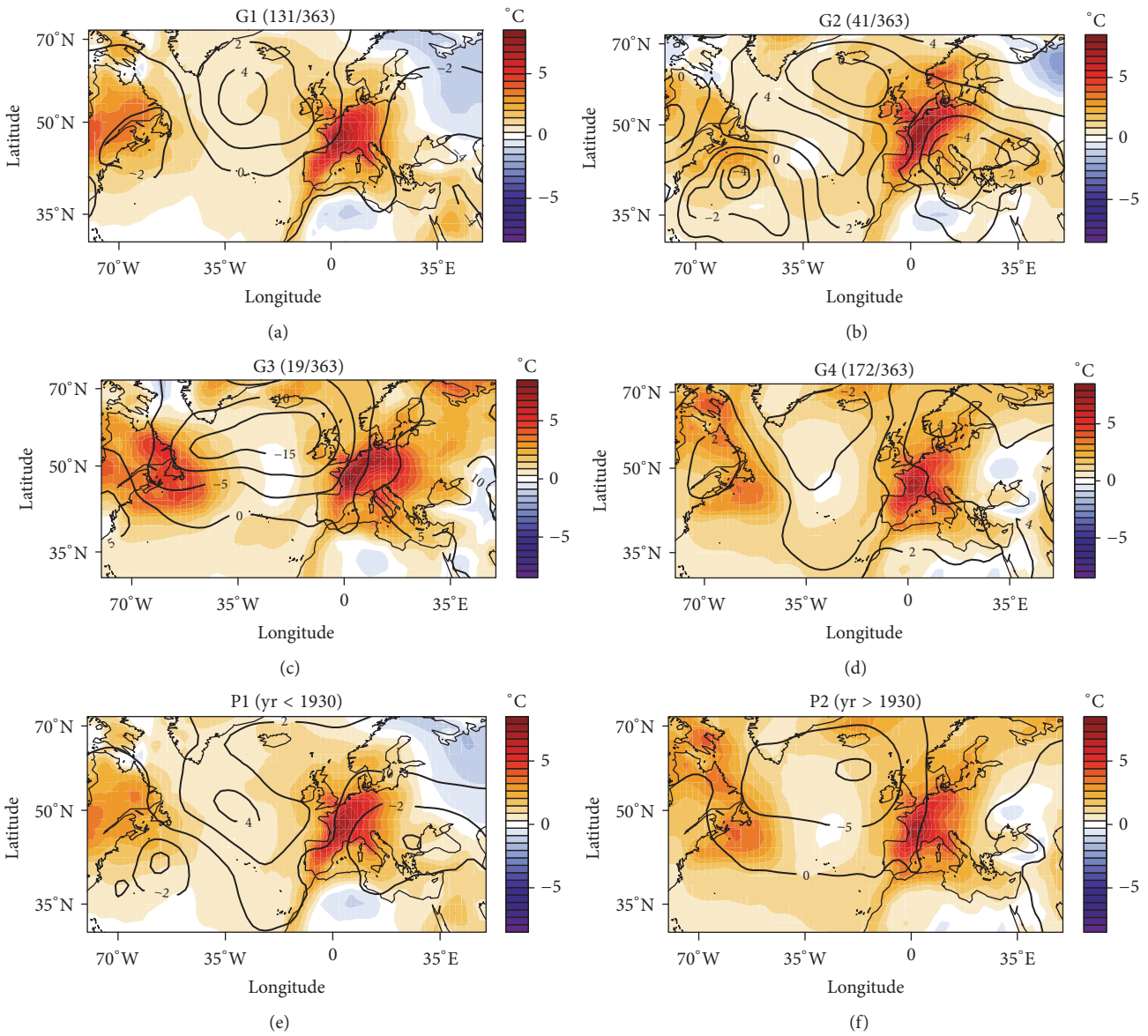

Figure 6: Composites of sea-level pressure (SLP) and surface temperature (SAT) anomalies during heatwaves events. In (a)–(d), composites SLP (hPa) and SAT (°C) anomalies for all the days during heatwaves events in each period, from G1 to G4; in (e), anomalies for all the days during heatwaves events before 1930 and (f) after 1930.

associated by AR (Figure 5(b)) and AL (Figure 5(d)) weather regimes have a frequency of 16% and 24%, respectively. The multidecadal variability in terms of frequency of weather regimes associated with warmest summers is also evident in the study of summer heatwave events. The summer average temperatures for Western Europe (Figure S5, supplementary material) show higher temperatures in the early and late time span. Those temperature anomalies are more evident once we apply high criteria to define heatwaves. There is a decrease in the occurrence of heatwave events during the first half of the 20th century being 1930–1950 the only period with some heatwave events that are more frequently associated with BLO regime. Although the late 19th century is dominated by BLO regime, each weather regime might induce a heatwave event. However, during the late 20th century and the beginning of 21st century, the NAO− regime is scarcely present during heatwave events, which are dominated by AL and, mainly, BLO. We also find that the longest events are associated with BLO regime (Figures 5(c) and 5(e)).

To shed more light on the circulation changes, we compute composites of SLP and surface temperature anomalies (Figure 6) during all the days of heatwave events detected in Figure 5 divided by periods (Table 1). Consistently with Figure 5, most of the heatwave events are concentrated in periods G1 (Figure 6(a)) and G4 (Figure 6(d)). There is a change also in the temperature patterns mainly in Northern and Eastern Europe but also in the East coast of North America and the Atlantic Ocean. Similar to G1, G2 (Figure 6(b)) has a NAO−

Table 1: Groups and periods used during the analysis of 20CRv2c (EM and 56 members of the ensemble).

Group	Years	Period
G1	1851–1890	P1
G2	1891–1930	
G3	1931–1970	P2
G4	1971–2010	

as the mean pressure pattern of the period of heatwave events. Although it is the period with scarce occurrence of heatwave events, G3 (Figure 6(c)) is dominated by a strong low pressure over the Atlantic ocean (with some influence of BLO over Europe) leading to an increase in temperature anomalies in both East Coast of North America and West Coast of Europe. Same exercise is repeated but taking into account the occurrence of heatwave events before 1930 (P1, Figure 6(e)) and after 1930 (P2, Figure 6(f)). The temperature pattern changes in pre- and post-1930 maps mainly in Greenland and the East Coast of North America and Europe (North and East). Pressure patterns for all the heatwave events before and after 1930 reproduce NAO− and BLO-AL, respectively, albeit weaker for the BLO regime which has a strong influence of AL regime (Figure S8, supplementary material). So, even if there is a change for NAO−, BLO is the one with a stronger change for short-term events, because it is the most representative pattern in heatwave events from 1930.

4. Conclusions

These results confirm that most heat events (either warmest summers and heatwaves in Western Europe) of the second half of the 20th century occurred when the Scandinavian Blocking weather regime dominated the North-Atlantic region, causing increasing temperatures and more frequent and longer heatwaves events (Figures 5 and S9). Our results also show that NAO− is more favorable to drive warm summers before 1930. This early period corresponds to the most frequent cooccurrence of this regime and heatwave events. Although the increasing temperature trends observed during blocking heatwave episodes could be attributed to secular climate change [29], the change in the dominating weather regimes may also be linked to the decadal variability of the atmospheric dynamics. Those findings are consistent with the results of Horton et al. [15], although we consider heatwaves on a finer spatial scale (Western Europe). The analysis of Hoffmann [30] is also complementary to ours, albeit on another region (Potsdam, Germany), whose temperature does not respond to the same atmospheric patterns. However, he found an increment of two new dominant wave-like patterns with more meridional oscillation, as we have seen for Western Europe at seasonal (Figures 1, S2, and S4) and subseasonal scales (Figure 5).

The robustness of our results is demonstrated by the use of 20CRv2c 56 ensemble members and other reanalysis datasets (see supplementary material) where we have found similar results. The dynamical analysis also suggests that there is an increase of negative correlations between warmest summers and the NAO− regime.

Although the information extracted in warmest summers and heatwaves is a priori different, our analysis shows similar results at different timescales. In terms of warmest summers, and although there are some evidence of a multidecadal variability of the atmospheric dynamic, NAO− was the most representative pattern up to 1930 and from 1930 on, BLO is the most representative one. For short time heat events, the most representative is BLO during the whole period but, as for the warmest summers, NAO− events are less frequent after 1930. BLO is associated with the longest and hottest heatwaves and yields an increasing trend, as outlined by Horton et al. [15].

Conflicts of Interest

The authors declare that there are no conflicts of interest regarding the publication of this paper.

Acknowledgments

M. Carmen Alvarez-Castro was supported by the Swedish Research Council Grant no. C0629701 (MILEX). Davide Faranda was supported by the ERC Grant no. 338965–A2C2. Pascal Yiou was supported by the European Union's Seventh Framework Programme Grant no. 607085–EUCLEIA. The authors thank G. Compo, for the help supported with data from members of 20CR reanalysis. 20CR and NCEP reanalysis data were provided by the NOAA/OAR/ESRL PSD, Boulder, Colorado, USA, and retrieved from https://climatedataguide.ucar.edu/climate-data/noaa-20th-century-reanalysis-version-2-and-2c and https://www.esrl.noaa.gov/psd/. ERA-20C reanalysis data were provided by the ECMWF (European Centre for Medium-Range Weather Forecasts), Reading, UK, from their website at http://apps.ecmwf.int/datasets/data/era20c-daily/.

Supplementary Materials

Figure S1: boxplots of absolute root mean square error by period and weather regime. Figure S2: relative long-term summer weather regime frequency over the North-Atlantic region and their dominance in warmest summers in Western Europe (1871–2016) using three reanalysis products (20CR, ERA20C, and NCEP). Figure S3: temperature anomalies maps for the warmest summers in Western Europe. Figure S4: 30 yr running correlations of summer mean temperatures and weather regime frequency in Western Europe. Figure S5: summer average temperatures (C) for Western Europe. (a) 20CR, (b) ERA20C, and (c) NCEP. Figure S6: dynamical representation of the warmest summers (same as g.3 in the main text) for ERA20C during 1900–2010. Figure S7: dominant weather regimes during summer heatwave events in Western Europe. Figure S8: mean SLP anomalies in heatwave events (20CRv2c EM) for each period. Figure S9: density plot of heatwave events. Table S1: absolute error of the root mean square deviation (AbsRMSE) of the truncated EOFs during the training period (NCEP: 1970–2010) by weather

regimes during summer in Western Europe (see also Figure S1). *(Supplementary Materials)*

References

[1] C. Schär and G. Jendritzky, "Climate change: hot news from summer 2003," *Nature*, vol. 432, pp. 559-560, 2017.

[2] P. Ciais, M. Reichstein, N. Viovy et al., "Europe-wide reduction in primary productivity caused by the heat and drought in 2003," *Nature*, vol. 437, no. 7058, pp. 529–533, 2005.

[3] M. Poumadere, C. Mays, S. L. Mer, and R. Blong, "The 2003 heat wave in France: dangerous climate change here and now," *Risk Analysis*, vol. 25, no. 6, pp. 1483–1494, 2005.

[4] J.-M. Robine, S. L. K. Cheung, S. Le Roy et al., "Death toll exceeded 70,000 in Europe during the summer of 2003," *Comptes Rendus Biologies*, vol. 331, no. 2, pp. 171–178, 2008.

[5] A. Wreford and W. N. Adger, "Adaptation in agriculture: historic effects of heat waves and droughts on UK agriculture," *International Journal of Agricultural Sustainability*, vol. 8, no. 4, pp. 278–289, 2010.

[6] C. Schär, D. Luthi, U. Beyerle, and E. Heise, "The soil-precipitation feedback: A process study with a regional climate model," *Journal of Climate*, vol. 12, no. 3, pp. 722–741, 1999.

[7] E. Fischer, S. Seneviratne, D. Luthi, and C. Schar, "Contribution of land-atmosphere coupling to recent European summer heat waves," *Geophysical Research Letters*, vol. 34, no. 6, 2007.

[8] R. Vautard, P. Yiou, F. D'Andrea et al., "Summertime European heat and drought waves induced by wintertime Mediterranean rainfall deficit," *Geophysical Research Letters*, vol. 34, no. 7, Article ID L07711, 2007.

[9] M. Zampieri, F. D'Andrea, R. Vautard, P. Ciais, N. De Noblet-Ducoudré, and P. Yiou, "Hot European summers and the role of soil moisture in the propagation of mediterranean drought," *Journal of Climate*, vol. 22, no. 18, pp. 4747–4758, 2009.

[10] B. Mueller and S. I. Seneviratne, "Hot days induced by precipitation deficits at the global scale," *Proceedings of the National Academy of Sciences*, vol. 109, no. 31, pp. 12398–12403, 2012.

[11] B. Quesada, R. Vautard, P. Yiou, M. Hirschi, and S. I. Seneviratne, "Asymmetric European summer heat predictability from wet and dry southern winters and springs," *Nature Climate Change*, vol. 2, no. 10, pp. 736–741, 2012.

[12] A. Jézéquel, P. Yiou, and S. Radanovics, "Role of circulation in European heatwaves using flow analogues," *Climate Dynamics*, 2017.

[13] P. M. Della-Marta, J. Luterbacher, H. von Weissenfluh, E. Xoplaki, M. Brunet, and H. Wanner, "Summer heat waves over western Europe 1880-2003, their relationship to large-scale forcings and predictability," *Climate Dynamics*, vol. 29, no. 2-3, pp. 251–275, 2007.

[14] M. Stefanon, F. D'Andrea, and P. Drobinski, "Heatwave classiffication over Europe and the Mediterranean region," *Environmental Research Letters*, vol. 7, no. 1, Article ID 014023, 2012.

[15] D. E. Horton, N. C. Johnson, D. Singh et al., "Contribution of changes in atmospheric circulation patterns to extreme temperature trends," *Nature*, vol. 522, no. 7557, pp. 465–469, 2015.

[16] G. P. Compo, J. S. Whitaker, P. D. Sardeshmukh et al., "The twentieth century reanalysis project," *Quarterly Journal of the Royal Meteorological Society*, vol. 137, no. 654, pp. 1–28, 2011.

[17] E. Kalnay, M. Kanamitsu, R. Kistler et al., "The NCEP/NCAR 40-year reanalysis project," *Bulletin of the American Meteorological Society*, vol. 77, no. 3, pp. 437–471, 1996.

[18] P. Poli et al., The data assimilation system and initial performance evaluation of the ecmwf pilot reanalysis of the 20th-century assimilating surface observations only (ERA-20C), ECMWF ERA Rep 14: 59.

[19] P. Yiou, K. Goubanova, Z. X. Li, and M. Nogaj, "Weather regime dependence of extreme value statistics for summer temperature and precipitation," *Nonlinear Processes in Geophysics*, vol. 15, no. 3, pp. 365–378, 2008.

[20] P.-A. Michelangeli, R. Vautard, and B. Legras, "Weather regimes: recurrence and quasi stationarity," *Journal of the Atmospheric Sciences*, vol. 52, no. 8, pp. 1237–1256, 1995.

[21] S. Corti, F. Molteni, and T. N. Palmer, "Signature of recent climate change in frequencies of natural atmospheric circulation regimes," *Letters to Nature*, vol. 398, no. 6730, pp. 799–802, 1999.

[22] C. Cassou, L. Terray, and A. S. Phillips, "Tropical Atlantic influence on European heat waves," *Journal of Climate*, vol. 18, no. 15, pp. 2805–2811, 2005.

[23] A. Katok and B. Hasselblatt, *Introduction to the modern theory of dynamical systems*, vol. 54, Cambridge University Press, 1997.

[24] E. N. Lorenz, "Dimension of weather and climate attractors," *Nature*, vol. 353, no. 6341, pp. 241–244, 1991.

[25] M. D. Chekroun, E. Simonnet, and M. Ghil, "Stochastic climate dynamics: Random attractors and time-dependent invariant measures," *Physica D: Nonlinear Phenomena*, vol. 240, no. 21, pp. 1685–1700, 2011.

[26] M. Casdagli, S. Eubank, J. D. Farmer, and J. Gibson, "State space reconstruction in the presence of noise," *Physica D: Nonlinear Phenomena*, vol. 51, no. 1–3, pp. 52–98, 1991.

[27] P. A. Stott, D. A. Stone, and M. R. Allen, "Human contribution to the European heatwave of 2003," *Nature*, vol. 432, no. 7017, pp. 610–614, 2004.

[28] G. A. Meehl and C. Tebaldi, "More intense, more frequent, and longer lasting heat waves in the 21st century," *Science*, vol. 305, no. 5686, pp. 994–997, 2004.

[29] D. Coumou, V. Petoukhov, S. Rahmstorf, S. Petri, and H. J. Schellnhuber, "Quasi-resonant circulation regimes and hemispheric synchronization of extreme weather in boreal summer," *Proceedings of the National Acadamy of Sciences of the United States of America*, vol. 111, no. 34, pp. 12331–12336, 2014.

[30] P. Hoffmann, "Enhanced seasonal predictability of the summer mean temperature in Central Europe favored by new dominant weather patterns," *Climate Dynamics*, 2017.